Dalton Transactions

Cite this: *Dalton Trans.*, 2012, **41**, 10970

www.rsc.org/dalton

PAPER

Tin(IV) and lead(IV) complexes with a tetradentate redox-active ligand†

Alexandr V. Piskunov,*[a] Olesya Yu. Trofimova,[a] Georgy K. Fukin,[a] Sergei Yu. Ketkov,[a] Ivan V. Smolyaninov[b] and Vladimir K. Cherkasov[a]

Received 22nd March 2012, Accepted 25th April 2012
DOI: 10.1039/c2dt30656e

The coordination chemistry of a tetradentate redox-active ligand, glyoxal-bis(2-hydroxy-3,5-di-*tert*-butylanil) (H_2L), was investigated with the diorganotin(IV) and diphenyllead(IV) moieties. Complexes R_2SnL (R = Me (**1**), Et (**2**), ^{t}Bu (**3**), Ph (**4**)) and Ph_2PbL (**5**) have been prepared and characterized. The molecular structures of compounds **1**, **3** and **5** have been determined by single crystal X-ray diffraction. The diamagnetic octahedral complexes bear a tetradentate *O*,*N*,*N*,*O* redox-active ligand with a nearly planar core. Complexes **1–5** demonstrate solvatochromism in solution. The CV of complexes **1–5** reveals four one-electron redox processes. The spin density distribution in the chemically generated cations and anions of **1–5** was studied by X-band EPR spectroscopy. The experimental data agree well with the results of DFT calculations of electronic structures for **1**, its pyridine adduct **1·Py**, cation $\mathbf{1}^+$ and anion $\mathbf{1}^-$.

Introduction

The chemistry of metal complexes with redox-active *o*-quinonato and *o*-iminoquinonato ligands has been extensively developed over the last forty years. The most important features of this chemistry based on transition metals have been collected in several reviews.[1] The chemistry of non-transition metal complexes with redox-active ligands has progressed in recent years.[2] Such types of ligands can reversibly accept one, two, or more electrons without loss of coordination to the metal. Thus a redox-active ligand bonded to a main-group-metal ion is able to reduce or oxidize a substrate coordinated to the metal. It is possible to simulate the specific reactivity of transition-metal coordination and organometallic compounds by non-transition-metal derivatives by including a redox-active ligand in a main-group-metal complex.[3] Tetradentate redox-active ligands are of special interest due to their ability to form a more extended range of redox and spin states. Five oxidation levels have been confirmed for metal complexes based on *N*,*N*′-bis(3,5-di-*tert*-butyl-2-hydroxyphenyl)-1,2-phenylenediamine.[4] Recently the dianion of *cis*-glyoxalbis(2-mercaptoanil) (*cis*-gma) was shown to be a redox-active tetradentate ligand. The diimine fragment of *cis*-gma can be reduced by one electron to form a monoradical trianionic ligand which has been experimentally characterized as an iron coordinated species.[5] Not long ago the cobalt(III) derivative with the dianion of *cis*-glyoxalbis(2-hydroxyanil) (*cis*-gha) was examined in the course of redox activity of the ligand moiety.[6] The sterically hindered tetra-*tert*-butyl substituted analogue of *cis*-gha – glyoxal-bis(2-hydroxy-3,5-di-*tert*-butylanil) (H_2L) – has been known since 1964[7] but its coordination chemistry has not been explored adequately to date. This type of ligand in its deprotonated form may potentially be involved in metal complexes in five different redox states (Scheme 1). The dianion (L^{-2}) and the trianion (L^{-3}) forms have a number of resonance structures. The neutral (L^0) and the tetraanion (L^{-4}) forms are diamagnetic while the monoanion (L^{-1}) and the trianion (L^{-3}) are radicals. In addition, the dianion (L^{-2}) can exist both in singlet (L^{-2A}, L^{-2B}) and triplet (L^{-2C}) states. The first attempts to synthesize metal derivatives with the deprotonated form of H_2L were performed by Wieghardt and co-workers.[8] The nickel(II) complex $Ni(HL)_2$ containing two tridentate mono-deprotonated HL ligands was prepared. Unfortunately the authors[8] were unable to obtain metal derivatives with the tetradentate form of this ligand.

In the present study we have synthesized diorganotin(IV) and diphenyllead(IV) complexes containing the tetradentate dianion of glyoxal-bis(2-hydroxy-3,5-di-*tert*-butylanil), and examined their molecular and electronic structure and activity in redox processes.

Experimental

General

The infrared spectra of the complexes in the 4000–400 cm^{-1} range were recorded on an FSM 1201 Fourier-IR spectrometer in

[a]*G.A. Razuvaev Institute of Organometallic Chemistry of the Russian Academy of Sciences, Tropinina str. 49, 603950 Nizhny Novgorod, Russia. E-mail: pial@iomc.ras.ru; Fax: +78314 627497; Tel: +7 8314 627682*
[b]*Southern Scientific Centre of the Russian Academy of Sciences, Toxicology Research Group, Tatischeva str. 16, 414025 Astrakhan, Russia. E-mail: thiophen@mail.ru; Fax: +78512 250923; Tel: +7 8512 553651*

†Electronic supplementary information (ESI) available: Optimized coordinates for *cis*-H_2L, *trans*-H_2L, **1**, **1·Py**, $\mathbf{1}^+$ and $\mathbf{1}^-$. CCDC reference numbers 872115–872117 for complexes **1**, **3** and **5** respectively. For ESI and crystallographic data in CIF or other electronic format see DOI: 10.1039/c2dt30656e

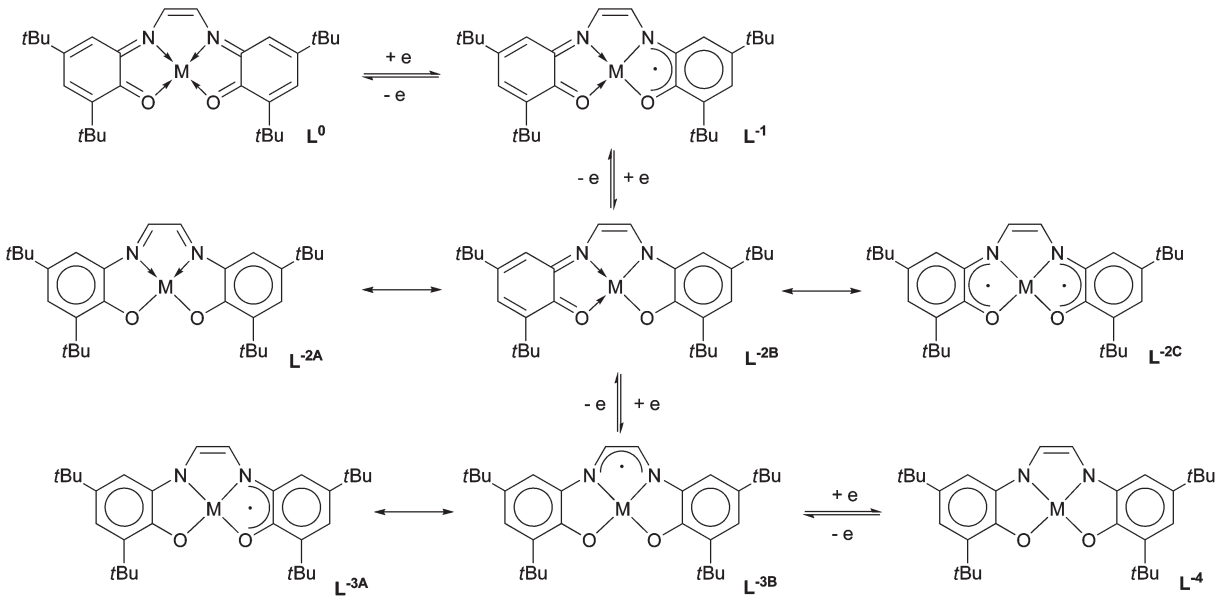

Scheme 1 The possible redox states and resonance structures for the L ligand in the metal complexes.

nujol. NMR spectra were recorded using a Bruker DPX-200 spectrometer and a Bruker Avance III 400 MHz instrument with Me_4Si as an internal standard. UV-Vis spectra were recorded on a Perkin-Elmer λ 25 spectrometer. EPR investigations were carried out using a Bruker EMX (working frequency ~ 9.75 GHz) spectrometer. The g_i values were determined using DPPH as the reference (g_i = 2.0037). HFS constants were obtained by simulation with the WinEPR SimFonia Software (Bruker).

Electrochemical studies were carried out using an IPC-Pro potentiostat in three-electrode mode. The stationary glassy carbon (d = 2 mm) disk was used as working electrode, and the auxiliary electrode was a platinum-flag electrode. The reference electrode was Ag/AgCl/KCl (sat.) with a watertight diaphragm and ferrocene was added as an internal standard ($E_{Fc+/Fc}$ = 0.42 V *vs.* Ag/AgCl). All measurements were carried out in CH_2Cl_2 under argon. The samples were dissolved in the pre-deaerated solvent. The scan rate was 200 mV s^{-1}. The supporting electrolyte 0.1 M Bu_4NClO_4 (99%, "Acros") was twice recrystallized from aqueous EtOH and then it was dried in vacuum (48 h). The elemental analysis was made using Elemental Analyzer Euro EA 3000 instrument.

Reagents were purchased from Aldrich. H_2L was synthesised according to the reported procedure.[4d] Solvents were purified following standard methods.[9] Organotin(IV) chlorides and diphenyllead dichloride were synthesized according to known methods.[10] All experiments concerning reduction and oxidation of complexes were carried out under conditions excluding oxygen and moisture.

X-ray crystallographic study of 1, 3 and 5

Intensity data for **1**, **3** and **5** were collected at 100 K on a Bruker Smart Apex diffractometer with graphite monochromated Mo-K_α radiation (λ = 0.71073 Å) in the φ–ω scan mode (ω = 0.3°, 10 sec on each frame). The intensity data were integrated by the SAINT program.[11] SADABS[12] was used to perform area-detector scaling and absorption corrections. The structures were solved by direct methods and were refined on F^2 using all reflections with the SHELXTL package.[13] All non-hydrogen atoms were refined anisotropically. All hydrogen atoms in **1**, **3** and **5** were placed in calculated positions and were refined in the riding model. The crystal data collection and structure refinement data are listed in Table 1.

Density functional theory calculations

DFT calculations were performed with the GAUSSIAN 03[14] program package using the B3LYP/DGDZVP (complexes **1**, **1+**, **1−** and **1·Py**) and B3LYP/6-31G(d) (*cis*-H_2L and *trans*-H_2L) levels of theory. The absence of imaginary frequencies after the optimization procedure suggests that the molecular geometries correspond to the energy minima.

Synthesis

General procedure for the preparation of complexes 1–5. An equimolar mixture of diorganotin dichloride (or diphenyllead dichloride) and H_2L was suspended in methanol (50 ml) under aerobic conditions. The addition of Et_3N (0.5 ml) led to the homogenization and the solutions became dark green. The reaction mixture was stirred for 30 min and a dark colored solid precipitated. The crystalline samples of complexes **1–5** were collected by filtration and washed with 5 ml of methanol.

Me_2SnL^2 (1). 0.46 g (1 mmol) of H_2L and 0.22 g (1 mmol) of Me_2SnCl_2. X-ray suitable crystals of **$1\cdot CH_2Cl_2$** were obtained from a CH_2Cl_2–methanol mixture. The total yield of the complex is 0.34 g (56%).

Anal. calc for $C_{32}H_{48}SnN_2O_2$ C, 62.86; H, 7.91; Sn, 19.41; N, 4.58%. Found: C, 62.53; H, 7.98; Sn, 19.52; N, 4.54%. ^{1}H NMR (400 MHz, $CDCl_3$, 293 K, δ (ppm), J/Hz): 0.61 (s, 6H, J (^{119}Sn-^{1}H) = 102.6, Sn-CH_3), 1.33, (s, 18H, *t*-Bu), 1.41 (s,

Table 1 The crystal data collection and structure refinement data for complexes **1**, **3** and **5**

Complex	**1·CH_2Cl_2**	**3**	**5·CH_2Cl_2**
Empirical formula	$C_{33}H_{50}Cl_2SnN_2O_2$	$C_{38}H_{60}SnN_2O_2$	$C_{43}H_{54}Cl_2PbN_2O_2$
Formula weight	696.34	695.57	908.97
T (K)	100(2)	100(2)	100(2)
Wavelength (Å)	0.71073	0.71073	0.71073
Crystal system	Monoclinic	Monoclinic	Triclinic
Space group	$P2_{1/c}$	$P2_{1/c}$	$P\bar{1}$
a (Å)	10.9657(4)	16.2139(5)	10.1974(3)
b (Å)	18.2113(6)	25.7750(8)	13.8984(4)
c (Å)	17.0576(6)	18.4703(5)	15.4418(4)
α (°)	90	90	69.3860(10)
β (°)	98.1810(10)	103.8960(10)	80.3170(10)
γ (°)	90	90	89.5930(10)
Volume (Å^3)	3371.7(2)	7493.1(4)	2016.00(10)
Z	4	8	2
Density (calculated) [g cm^{-3}]	1.372	1.233	1.497
Absorption coefficient (mm^{-1})	0.947	0.714	4.354
Crystal size (mm)	0.20 × 0.05 × 0.04	0.65 × 0.60 × 0.41	0.42 × 0.18 × 0.04
Θ range for data collection [°]	2.18–26.00	1.58–27.00	2.27–26.50
Reflections collected	28 608	48 606	12 739
Independent reflections	6605 [R(int) = 0.0498]	16 333 [R(int) = 0.0195]	8283 [R(int) = 0.0114]
Completeness (to Θ)	99.6 (26.00)	99.9% (27.00)	99.1% (26.50)
Absorption correction	Semi-empirical from equivalents	Semi-empirical from equivalents	Semi-empirical from equivalents
Max. and min. transmission	0.9631 and 0.8332	0.7584 and 0.6539	0.8451 and 0.2621
Refinement method	Full-matrix least-squares on F^2	Full-matrix least-squares on F^2	Full-matrix least-squares on F^2
Data/restraints/parameters	6605/0/375	16 333/0/811	8283/0/471
Final R indices [$I > 2\sigma(I)$]	R_1 = 0.0321, wR_2 = 0.0674	R_1 = 0.0284, wR_2 = 0.0680	R_1 = 0.0200, wR_2 = 0.0513
R indices (all data)	R_1 = 0.0523, wR_2 = 0.0725	R_1 = 0.0362, wR_2 = 0.0711	R_1 = 0.0216, wR_2 = 0.0519
Goodness-of-fit on F^2	1.000	1.064	1.068
Largest diff. peak and hole [e Å^{-3}]	0.848 and −0.520	1.345 and −0.703	1.616 and −1.312

18H, *t*-Bu), 7.22 (d, 2H, 2.09, aromatic), 7.29 (d, 2H, 2.09, aromatic), 8.35 (s, 2H, J (^{119}Sn–^{1}H) = 22.40, CH). ^{13}C NMR (100 MHz, $CDCl_3$, 293 K, δ (ppm), J/Hz): 6.77 (Sn-CH_3, J (^{119}Sn–^{13}C) = 929.5), 29.11, 31.18 (CH_3(*t*-Bu)), 34.51, 35.47 (C(*t*-Bu)), 109.56, 128.33, 129.03, 133.01, 137.71, 141.88 (aromatic), 164.65 (C═N, J (^{119}Sn–^{13}C) = 26.6). ^{119}Sn NMR (149 MHz, $CDCl_3$, 293 K, δ (ppm)): −254.90. ^{1}H NMR (400 MHz, d-Py, 293 K, δ (ppm), J/Hz): 0.65 (s, 6H, J (^{119}Sn–^{1}H) = 114.9, Sn–CH_3), 1.30, (s, 18H, *t*-Bu), 1.54 (s, 18H, *t*-Bu), 7.63 (d, 2H, 2.19, aromatic), 8.68 (s, 4H, aromatic and CH). ^{13}C NMR (100 MHz, d-Py, 293 K, δ (ppm), J/Hz): 12.31 (Sn–CH_3, J (^{119}Sn–^{13}C) = 1205.7), 29.33, 31.31 (CH_3(*t*-Bu)), 34.28, 35.39 (C(*t*-Bu)), 110.81, 127.30, 130.55, 136.13, 136.24, 140.79 (aromatic), 163.83 (C═N, J (^{119}Sn-^{13}C) = 26.7). ^{119}Sn NMR (149 MHz, d-Py, 293 K, δ (ppm)): −417.97. IR (KBr) cm^{-1}: 1562(m), 1520(m), 1516(s), 1483(m), 1408(s), 1379(s), 1361(s), 1341(s), 1288(m), 1266(m), 1253(s), 1239(s), 1200(s), 1158(s), 1116(m), 1071(w), 1038(m), 1023(m), 1009 (w), 968(w), 932(w), 910(s), 897(w), 843(s), 832(w), 780(w), 748(w), 727(m), 636(m), 583(m), 570(m), 527(m). λ_{max} (toluene, 293 K)/nm 432 (ε/dm^3 mol^{-1} cm^{-1} 6500), 789 (22 100). λ_{max} (acetonitrile, 293 K)/nm 418 (ε/dm^3 mol^{-1} cm^{-1} 8600), 738 (24 000). λ_{max} (THF, 293 K)/nm 415 (ε/dm^3 mol^{-1} cm^{-1} 8200), 723 (23 400). λ_{max} (MeOH, 293 K)/nm 409 (ε/dm^3 mol^{-1} cm^{-1} 7200), 706 (19 500). λ_{max} (pyridine, 293 K)/nm 399 (ε/dm^3 mol^{-1} cm^{-1} 9000), 679 (23 400).

Et_2SnL^2 (2). 0.46 g (1 mmol) of H_2L and 0.25 g (1 mmol) of Et_2SnCl_2. The total yield of the complex is 0.27 g (42%).

Anal. calc for $C_{34}H_{52}SnN_2O_2$ C, 63.86; H, 8.20; Sn, 18.56; N, 4.38%. Found: C, 63.75; H, 8.27; Sn, 18.62; N, 4.33%. ^{1}H NMR (400 MHz, $CDCl_3$, 293 K, δ (ppm), J/Hz): 0.87 (t, 6H, J (^{119}Sn-^{1}H) = 155.6, CH_3(Et)), 1.32 (s, 18H, *t*-Bu), 1.33 (quartet, 4H, CH_2(Et)), 1.41 (s, 18H, *t*-Bu), 7.20 (d, 2H, 2.14, aromatic), 7.26 (d, 2H, 2.14, aromatic), 8.37 (s, 2H, J (^{119}Sn–^{1}H) = 17.20, CH). ^{13}C NMR (100 MHz, $CDCl_3$, 293 K, δ (ppm)): 9.72 (CH_3(Et)), 19.24 (CH_2(Et)), 29.16, 31.20 (CH_3(*t*-Bu)), 34.50, 35.40 (C(*t*-Bu)), 109.39, 128.13, 129.80, 133.10,137.47,141.57 (aromatic), 165.54 (C═N). ^{119}Sn NMR (149 MHz, $CDCl_3$, 293 K, δ (ppm)): −270.92. IR (KBr) cm^{-1}: 1561(m), 1533(m), 1516(s), 1403(s), 1361(s), 1343(m), 1285(m), 1266(m), 1251(s), 1236(s), 1200(m), 1158(s), 1115(s), 1072(m), 1036(m), 1022 (m), 1008(m), 966(w), 931(w), 909(s), 841(m), 830(w), 779(w), 748(w), 732(m), 669(w), 635(m), 582(w), 528(m). λ_{max} (toluene, 293 K)/nm 432 (ε/dm^3 mol^{-1} cm^{-1} 7200), 787 (24 900).

***t*-Bu_2SnL^2 (3).** 0.46 g (1 mmol) of H_2L and 0.30 g (1 mmol) of *t*-Bu_2SnCl_2. X-ray suitable crystals were obtained from a CH_2Cl_2–methanol mixture. The total yield of the complex is 0.45 g (65%).

Anal. calc for $C_{38}H_{60}SnN_2O_2$ C, 65.61; H, 8.69; Sn, 17.07; N, 4.03%. Found: C, 65.54; H, 8.76; Sn, 17.16; N, 4.01%. ^{1}H NMR (400 MHz, $CDCl_3$, 293 K, δ (ppm), J/Hz): 1,08 (s, 18H, J (^{119}Sn–^{1}H) = 129.9, *t*-Bu(Sn)), 1.31 (s, 18H, *t*-Bu), 1.47 (s, 18H, *t*-Bu), 7.15 (d, 2H, 2.08, aromatic), 7.25 (d, 2H, 2.08, aromatic), 8.34 (s, 2H, J (^{119}Sn–^{1}H) = 12.55, CH). ^{13}C NMR (100 MHz, $CDCl_3$, 293 K, δ (ppm)): 29.55, 30.05, 31.25 (CH_3(*t*-Bu)), 34.47, 35.37, 43.84 (C(*t*-Bu)), 109.17, 128.05, 131.22, 132.42, 137.41, 140.90 (aromatic), 166.70 (C═N). ^{119}Sn NMR (149 MHz, $CDCl_3$, 293 K, δ (ppm)): −344.58. IR (KBr) cm^{-1}: 1559(m), 1530(m), 1514(s), 1405(s), 1359(s), 1335(s), 1284(s),

1264(m), 1250(m), 1233(s), 1197(s), 1155(s), 1117(s), 1066(m), 1037(m), 1023(m), 1009(m), 966(w), 928(w), 909(s), 894(w), 845(s), 828(w), 781(w), 746(w), 730(m), 671(w), 637(m), 584 (w), 527(m). λ_{max} (toluene, 293 K)/nm 434 (ε/dm^3 mol^{-1} cm^{-1} 7800), 800 (25 900).

Ph_2SnL^2 (4). 0.46 g (1 mmol) of H_2L and 0.34 g (1 mmol) of Ph_2SnCl_2. The total yield of the complex is 0.29 g (40%).

Anal. calc for $C_{42}H_{52}SnN_2O_2$ C, 68.58; H, 7.13; Sn, 16.14; N, 3.81%. Found: C, 68.52; H, 7.19; Sn, 16.25; N, 3.78%. ^{1}H NMR (400 MHz, $CDCl_3$, 293 K, δ (ppm), *J*/Hz): 1,34 (s, 18H, *t*-Bu), 1.48 (s, 18H, *t*-Bu), 7.14 (m, 6H, *m*-*p*-H(Sn-Ph)), 7.19 (d, 2H, 2.20, aromatic), 7.40 (d, 2H, 2.20, aromatic), 7.54 (dd, 4H, 1.20, 8.04, *J* (^{119}Sn–^{1}H) = 100.14, *o*-H(Sn-Ph)), 8.31 (s, 2H, *J* (^{119}Sn–^{1}H) = 24.40, CH). ^{13}C NMR (100 MHz, $CDCl_3$, 293 K, δ (ppm)): 29.45, 31.21 (CH_3(*t*-Bu)), 34.55, 35.46 (C(*t*-Bu)), 109.99, 128.06, 128.74, 129.05, 129.89, 133.38, 136.04, 138.34, 141.19, 146.05 (aromatic), 165.33 (C═N). ^{119}Sn NMR (149 MHz, $CDCl_3$, 293 K, δ (ppm)): −421.30. IR (KBr) cm^{-1}: 1585(s), 1540(w), 1524(s), 1478(s), 1430(m), 1406(m), 1377(s), 1359(s), 1326(s), 1319(s), 1280(s), 1259(s), 1234(s), 1199(s), 1160(s), 1117(s), 1078(w), 1063(m), 1038(s), 1026(m), 1011(s), 960(w), 930(w), 910(s), 872(m), 860(m), 846(m), 831(m), 779 (w), 740(s), 694(s), 658(w), 640(w), 590(w), 569(m), 529(m). λ_{max} (toluene, 293 K)/nm 429 (ε/dm^3 mol^{-1} cm^{-1} 7500), 758 (19 300).

Ph_2PbL^2 (5). 0.46 g (1 mmol) of H_2L and 0.43 g (1 mmol) of Ph_2PbCl_2. X-ray suitable crystals of **5·CH_2Cl_2** were obtained from a CH_2Cl_2–methanol mixture. The total yield of the complex is 0.57 g (69%).

Anal. calc for $C_{42}H_{52}PbN_2O_2$ C, 61.21; H, 6.36; Pb, 25.14; N, 3.40%. Found: C, 61.20; H, 6.42; Pb, 25.19; N, 3.36%. ^{1}H NMR (400 MHz, $CDCl_3$, 293 K, δ (ppm), *J*/Hz): 1.31 (s, 18H, *t*-Bu), 1.48 (s, 18H, *t*-Bu), 7.08 (d, 2H, 2.40, aromatic), 7.29 (m, 6H, *m*-*p*-H(Pb-Ph))7.34 (d, 2H, 2.40, aromatic), 7.89 (dd, 4H, 1.20, 8.13, *o*-H(Pb-Ph)), 8.31 (s, 2H, CH). ^{13}C NMR (100 MHz, $CDCl_3$, 293 K, δ (ppm)): 29.47, 31.23 (CH_3(*t*-Bu)), 34.38, 35.43 (C(*t*-Bu)), 110.65, 128.36, 129.81, 129.87, 131.91. 135.47, 135.77, 136.55, 142.68, 162.14 (aromatic), 167.05 (C═N). IR (KBr) cm^{-1}: 1576.1(s), 1531.0(w), 1516.0(s), 1481.5(s), 1403.4(s), 1380.9(s), 1362.9(m), 1329.9(m), 1280.4 (m), 1260.9(s), 1247.3(s), 1233.8(s), 1199.3(s), 1151.3(s), 1121.3(m), 1089.7(w), 1064.2(m), 1025.2(m), 1016.2(m), 1008.7(m), 993.7(m), 963.7(w), 933.6(w), 909.6(s), 896.1(w), 878.1(w), 858.6(m), 849.6(m), 828.6(w), 780.5(w), 740.0(m), 726.5(s), 686.0(m), 631.9(m), 580.9(w), 523.9(m), 507.4(w). λ_{max} (toluene, 293 K)/nm 420 (ε/dm^3 mol^{-1} cm^{-1} 7500), 770 (22 200). λ_{max} (Py, 293 K)/nm 402 (ε/dm^3 mol^{-1} cm^{-1} 7000), 707 (17 400).

Results and discussion

Synthesis

Interest in the synthesis of complexes containing the glyoxal-bis-(2-hydroxy-3,5-di-*tert*-butylanil) was caused by the necessity to establish the potential of this ligand to be involved in redox transformations. The decision to obtain complexes with group 14 elements was made based on two reasons. The redox inactive metals make it possible to observe pure redox behavior of the coordinated ligand which is not complicated with oxidation or reduction of the metallic center. In addition, glyoxal-bis(2-hydroxy-3,5-di-*tert*-butylanil) is known to prefer tridentate coordination with the small cation of nickel.[4] A large coordination sphere of diorganotin or diorganolead dications should provide the tetradentate coordination of the organic ligand.

The reaction of H_2L with organometallic chlorides (ratio 1 : 1) in methanol in the presence of triethylamine at room temperature resulted in the formation of dark colored precipitates of complexes **1–5** (Scheme 2).

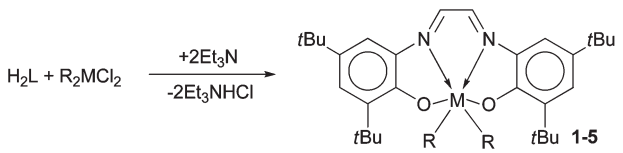

M=Sn; R=Me(**1**), Et(**2**), *t*Bu(**3**), Ph(**4**); M=Pb; R=Ph(**5**)

Scheme 2 Synthesis of **1–5**.

X-ray structures

The molecular structures of complexes **1**, **3** and **5** were examined with X-ray diffraction analysis. X-ray suitable crystals of the complexes were obtained by prolonged crystallization from a CH_2Cl_2–methanol mixture. Crystals of complexes **1** and **5** have one CH_2Cl_2 solvated molecule per complex molecule. There are two crystallographically unique molecules in the asymmetric unit of **3** but their geometries around the metal center are similar and only one molecule is discussed. Fig. 1–3 show the molecular

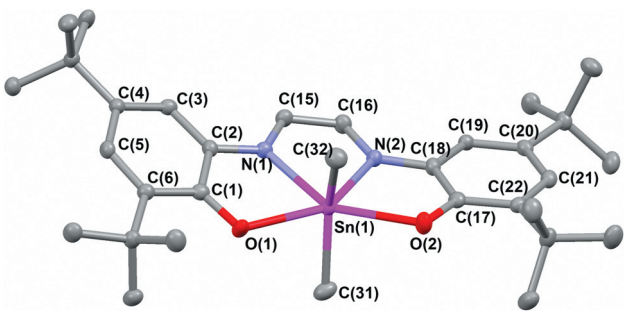

Fig. 1 The molecular structure of **1** with 50% ellipsoid probability. H atoms and the solvated CH_2Cl_2 molecule are omitted for clarity.

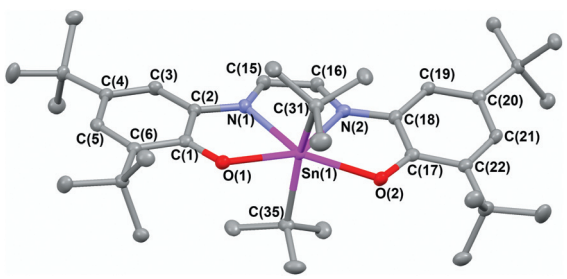

Fig. 2 The molecular structure of **3** with 50% ellipsoid probability. H atoms are omitted for clarity.

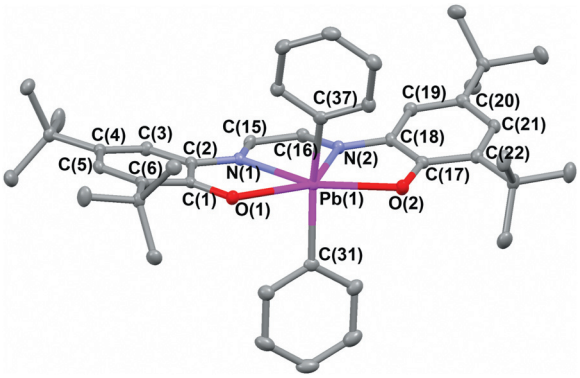

Fig. 3 The molecular structure of **5** with 50% ellipsoid probability. H atoms and the solvated CH_2Cl_2 molecule are omitted for clarity.

structures of **1**, **3** and **5** respectively. Selected bond lengths and angles for **1**, **3** and **5** are summarized in Table 2.

The distorted octahedral coordination sphere of the metals in complexes **1**, **3** and **5** is formed by two alkyl (or aryl) substituents and the tetradentate chelated L ligand. Oxygen and nitrogen atoms of the latter lie in the equatorial plane while the hydrocarbon fragments are in the apical positions. The tin (or lead) atoms are strongly deviated from the centre of the tetragon O(1)N(1)N(2)O(2). The geometry of the ONNO ligand in **1**, **3** and **5** is close to planar. The dihedral angles between the C(1)–C(6) and C(17)–C(22) rings are 24.62°, 12.32° and 20.39° for **1**, **3** and **5** respectively.

One of the chlorine atoms of the solvated CH_2Cl_2 molecule in **1** and **5** is disposed in the plane of the eleven membered metallocycle. The Sn···Cl and Pb···Cl distances in **1** and **5** are 3.977 Å and 3.396 Å respectively. Such Sn(Pb)···Cl distances allow to suppose the presence of van der Waals (vdW) interactions between these atoms. The sum of vdW radii for Sn and Cl (Pb and Cl) atoms is 4.0 Å (4.1 Å). This vdW contact is normal in **1** whereas it is significantly shortened in **5**. The C(Ph)PbC(Ph) angle (158.15(7)°) has a maximal value in comparison with analogous angles in **1** (144.75(10)°) and **3** (153.76(7)°) as a consequence. It should be noted that there is no solvated CH_2Cl_2 molecule in **3**. However the C(Bu^t)SnC(Bu^t) angle in **3** significantly exceeds the equivalent one in **1**. These observations suggest a weakness of the intermolecular Sn···Cl interactions in **1** and strength of the non-bonding interactions between the *tert*-butyl groups in **3**.

The bond distances in the glyoxal bridging unit of the L ligand in complexes **1**, **3** and **5** are very informative in establishing its electronic configuration. The C–C and C–N distances in a neutral diimine are known to be sharply different from those in a corresponding reduced diimine. The C–N and C–C distances in the neutral diimine coordinated to the tin atom are 1.27 and 1.47 Å respectively,[15] whereas the corresponding bond lengths in the diimine radical-anion are 1.32 and 1.40 Å.[16] The bond parameters of the glyoxal fragment in **1**, **3** and **5** are 1.301(3), 1.300(2), 1.298(2) Å and 1.419(3), 1.430(2), 1.437(3) Å for C–N and C–C respectively. They are close to those observed for the $[Co(gha)(PPh_3)_2]^+$ cation[6] and are intermediate between the values typical for neutral diimine and its radical-anion. It is important to note that complexes **1–5** exhibit C═N stretching vibrations at 1561–1585 cm^{-1} which is slightly less than the stretching frequency of a coordinated aldimine (>1600 cm^{-1})[17] indicating the elongation of the C═N bond in comparison with diazabutadienes. This effect can be explained by the additional conjugation of the diimine moiety π-system with the π-system of the phenolate parts of the ligand. Unfortunately there are no structural data for H_2L or any similar ligands. We have performed DFT calculations for H_2L. The *trans*-configuration appears to be 1.27 kcal mol^{-1} more stable than the *cis* geometry.

Table 2 Selected bond lengths (Å) and angles (°) for **1**, **3** and **5**

Bond[a]	1	3	5
M(1)–O(1)	2.2518(16)	2.2544(12)	2.4187(13)
M(1)–N(1)	2.2626(19)	2.2668(14	2.4196(16)
M(1)–O(2)	2.2649(16)	2.2707(12)	2.3522(14)
M(1)–N(2)	2.2523(19)	2.2626(14)	2.3749(15)
O(1)–C(1)	1.295(3)	1.301(2)	1.302(2)
O(2)–C(17)	1.308(3)	1.311(2)	1.307(2)
N(1)–C(15)	1.301(3)	1.300(2)	1.298(2)
N(1)–C(2)	1.386(3)	1.389(2)	1.387(2)
N(2)–C(16)	1.306(3)	1.305(2)	1.296(2)
N(2)–C(18)	1.388(3)	1.389(2)	1.392(2)
C(1)–C(2)	1.426(3)	1.433(2)	1.431(3)
C(1)–C(6)	1.439(3)	1.435(2)	1.444(3)
C(2)–C(3)	1.410(3)	1.404(2)	1.411(3)
C(3)–C(4)	1.371(3)	1.378(2)	1.369(3)
C(4)–C(5)	1.426(3)	1.413(2)	1.419(3)
C(5)–C(6)	1.372(3)	1.383(2)	1.378(3)
C(15)–C(16)	1.419(3)	1.430(2)	1.437(3)
C(17)–C(18)	1.422(3)	1.428(2)	1.427(3)
C(17)–C(22)	1.439(3)	1.443(2)	1.437(3)
C(18)–C(19)	1.405(3)	1.406(2)	1.403(3)
C(19)–C(20)	1.372(3)	1.372(2)	1.380(3)
C(20)–C(21)	1.415(3)	1.422(2)	1.412(3)
C(21)–C(22)	1.377(3)	1.375(3)	1.383(3)
M(1)–C(31)	2.115(2)	2.2003(18)	2.180(2)
M(1)–C(32)	2.122(2)	—	—
M(1)–C(35)	—	2.2009(18)	—
M(1)–C(37)	—	—	2.179(2)
Angle			
C(31)–M(1)–C(32)	144.75(10)	—	—
C(31)–M(1)–C(35)	—	153.76(7)	—
C(31)–M(1)–C(37)	—	—	158.15(7)
C(31)–M(1)–O(1)	83.47(8)	85.43(6)	88.49(6)
C(32)–M(1)–O(1)	85.05(8)	—	—
C(35)–M(1)–O(1)	—	86.96(6)	—
C(37)–M(1)–O(1)	—	—	85.00(6)
C(31)–M(1)–N(2)	102.37(8)	100.23(6)	99.71(6)
C(32)–M(1)–N(2)	107.03(9)	—	—
C(35)–M(1)–N(2)	—	100.74(6)	—
C(37)–M(1)–N(2)	—	—	99.49(6)
O(1)–M(1)–N(2)	142.20(6)	143.69(5)	135.75(5)
C(31)–M(1)–N(1)	110.22(9)	104.04(6)	96.13(6)
C(32)–M(1)–N(1)	97.26(9)	—	—
C(35)–M(1)–N(1)	—	97.36(6)	—
C(37)–M(1)–N(1)	—	—	100.51(6)
O(1)–M(1)–N(1)	71.20(6)	72.00(5)	67.29(5)
N(2)–M(1)–N(1)	71.78(7)	71.84(5)	68.61(5)
C(31)–M(1)–O(2)	85.25(9)	87.06(6)	87.50(6)
C(32)–M(1)–O(2)	86.01(8)	—	—
C(35)–M(1)–O(2)	—	84.69(6)	—
C(37)–M(1)–O(2)	—	—	89.67(6)
O(1)–M(1)–O(2)	146.12(6)	144.54(4)	155.10(4)
N(2)–M(1)–O(2)	71.53(6)	71.77(5)	69.13(5)
N(1)–M(1)–O(2)	142.46(6)	143.28(5)	137.59(5)

[a] M = Sn for **1** and **3**; M = Pb for **5**.

The calculated C–N and C–C distances of the glyoxal fragment in the free *trans*-H_2L ligand are 1.289 and 1.446 Å, respectively, which are very close to those obtained for complexes **1**, **3** and **5**.

On the other hand, the structural parameters of the L ligand show a quinoid-type distortion in the two aromatic phenolic rings. The C(3)–C(4) and C(5)–C(6) bond distances are shorter than the average bond distances of C(1)–C(2), C(2)–C(3), C(4)–C(5) and C(1)–C(6). The same trend is also evident in the other ring where both the C(19)–C(20) and C(21)–C(22) bonds are shorter than the other ones. The C–O distances are also shorter than the C–O bonds in reported tin(IV) *o*-amidophenolate complexes[18a,b] and are closer to those obtained for the corresponding *o*-iminosemiquinolate derivatives.[3e,18b–e] The above mentioned structural features indicate the importance of resonance structures L^{-2B} and L^{-2C} (Scheme 1) on consideration of complexes **1–5**.

Electronic spectra

The electronic absorption data of complexes **1–5** are summarized in Table 3 and shown in Fig. 4 for complex **1**. The spectrum of **1** appears to be dominated by two intense ligand-to-ligand charge transfers (LLCT). The positions of these bands were found to be strongly influenced by solvent. This influence is due to the coordination capability of the solvent molecule rather than its polarity. It is clear from the comparison of the spectra in acetonitrile (strongly polar and weak donor) and pyridine (strong donor and medium polarity) that the shift of the charge transfer bands is much larger in pyridine than in acetonitrile. The solutions of complexes **1–5** in toluene are green while in pyridine they are blue.

Table 3 Electronic spectra of complexes at 293 K

Complex	Solvent	λ_{max}, nm (ε, dm^3 mol^{-1} cm^{-1})
1	Toluene	423 (6500), 789 (22 100)
	Acetonitrile	418 (8600), 738 (24 000)
	THF	415 (8200), 723 (24 400)
	Methanol	409 (7200), 706 (19 500)
	Pyridine	399 (9000), 679 (23 400)
2	Toluene	432 (7200), 787 (24 900)
3	Toluene	434 (7800), 800 (25 900)
4	Toluene	429 (7500), 758 (19 300)
5	Toluene	420 (7500), 770 (22 200)
	Pyridine	402 (7000), 707 (17 400)

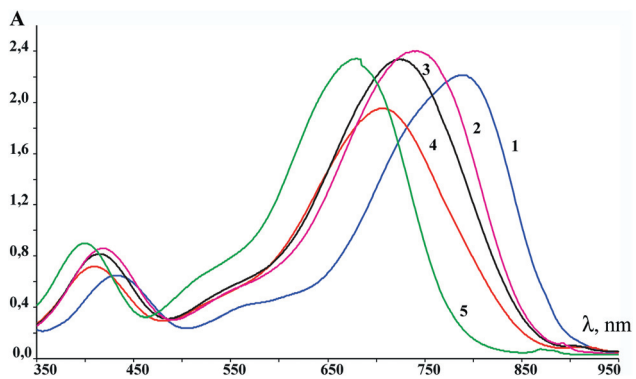

Fig. 4 UV-vis spectra of **1** in toluene (1), acetonitrile (2), THF (3), methanol (4) and pyridine (5). $C = 1 \times 10^{-4}$ M.

According to the structure of complexes **1**, **3** and **5** the metallic center has a vacant place between alkyl (or aryl) substituents which is sufficient for the coordination of an extra ligand. Such coordination has to be accompanied by an increase of the coordination number of the metal up to seven and an increase of the C–M–C angle. It is evidenced by the NMR spectroscopy experiments. A δ value in the range from −254.9 to −421.3 ppm for the ^{119}Sn NMR spectra was obtained for complexes **1–4** in $CDCl_3$. The chemical shifts are in agreement with the range of *ca.* −125 to −525 ppm reported for six-coordinated tin(IV) compounds.[19] It is well known that an increase in the coordination number of tin should give rise to a high field shift of δ (^{119}Sn).[20] Indeed the chemical shift δ (^{119}Sn) for complex **1** increases from −254.90 to −417.97 ppm when the ^{119}Sn NMR spectrum is recorded in Py-d_5. In addition the magnitude of the tin–carbon J coupling, ($^1J(^{119}Sn,^{13}C)$), depends linearly on the Me–Sn–Me angle in compliance with the known equation.[21] The Me–Sn–Me angle of complex **1** in the course of pyridine coordination increases by 30° as can be estimated from the differences between the $^1J(^{119}Sn,^{13}C)$ values for **1** recorded in $CDCl_3$ and Py-d_5 on the basis of this equation.[21]

Cyclic voltammetry

The electronic structure of compounds **1–5** was assessed by performing cyclic voltammetry in dichloromethane solution. The relatively high scan rate (200 mV s^{-1}) was chosen to increase the reversibility of the redox waves. The CV experiments with a lower scan rate (50 mV s^{-1}) were complicated with the adsorption–desorption processes. Fig. 5 displays the cyclic voltammogram (CV) of complex **1**. Electrochemical data for all complexes **1–5** are summarized in Table 4.

The CV of **1**, **2** and **4** displays four reversible one-electron transfer waves due to the change of the ligand redox states (Scheme 3). The redox potentials of complexes **1–4** are influenced by the nature of the hydrocarbon substituent bonded to the tin. The donor groups shift the position of $E_{1/2}$ into the cathodic region (**3** < **2** < **1**) while electron-withdrawing phenyls

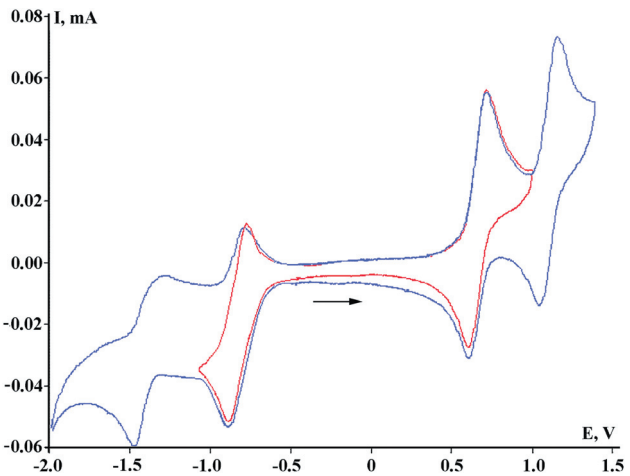

Fig. 5 CV of compound **1**.

Table 4 The electrochemical data[a] for complexes **1–5**

Complex	$E^{Red.1}{}_{1/2}$, V	$E^{Red.2}{}_{1/2}$, V	$E^{Ox.1}{}_{1/2}$, V	$E^{Ox.2}{}_{1/2}$, V
1	−0.83	−1.41	0.65	1.10
2	−0.88	−1.48	0.65	1.11
3	−0.88	−1.60[b]	0.63	1.32[b]
4	−0.70	−1.30	0.78	1.23
5	−0.89	−1.37[b]	0.62	0.98

[a] CH_2Cl_2 solution containing 0.1 M n-Bu_4NClO_4 supporting electrolyte, scan rate = 200 mV s^{-1}, *vs.* Ag/AgCl/KCl, C = 1–3 × 10^{-3} M, glassy carbon working electrode, Ar, 0.1 M Bu_4NClO_4. [b] The value of peak potential for irreversible process.

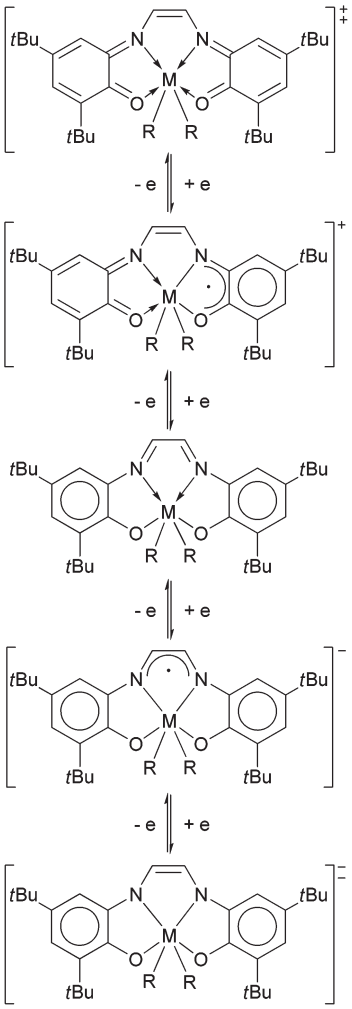

Scheme 3 Redox states of the complexes **1–5**.

(**4**) complicate the oxidation and shift the potentials in the anodic direction.

Complex **3** slightly differs from the other tin compounds. The *tert*-butyl substituent lead to the destabilization of doubly charged ions. The first cathodic process gives the anion which is relatively stable on the electrochemical time scale. The second one-electron reduction is irreversible and leads to the additional chemical transformations following the electrochemical stage. It is evidenced by the presence of additional oxidation waves on the reverse scan of the CV. A similar situation occurs in the anodic region. The first oxidation wave responds to the formation of the relatively stable cation (I_c/I_a = 0.45) while the second irreversible redox process ($E_{1/2}$ = 1.32 V) is shifted to the anodic region in comparison with **1**, **2** and **4**.

The additional one electron oxidation wave is observed at 1.45 V. This value is very close to the oxidation potential of sterically hindered *o*-iminobenzoquinones[22] and is responsible for the oxidation of the imine nitrogen atom in L^0. Two irreversible anodic processes at $E_{1/2}$ 1.32 and 1.45 V result in the destruction of **3** and the reversibility of the first anodic redox wave disappears on the reverse scan of the CV.

The CV of **5** displays four one-electron transfer waves. Both the anodic waves are reversible while only the first redox process in the cathodic region is reversible. The nature of the metal ion has an effect on the values of the redox potentials. They are shifted into the cathodic region for complex **5** in comparison with the tin complex **4**.

The cations and anions of complexes **1–5** were generated chemically by oxidation with $AgBF_4$ or reduction with metallic potassium respectively. The obtained CH_2Cl_2 (for cations) and THF (for anions) solutions were examined with X-band EPR spectroscopy.

The EPR spectra of cations $\mathbf{1}^+$–$\mathbf{5}^+$ are wide singlets (ΔH = 2–3 G) with satellite splitting due to the interaction of unpaired electrons with the magnetic isotopes of tin (^{117}Sn (7.68%, I = 1/2, μ_N = 1.000), ^{119}Sn (8.58%, I = 1/2, μ_N = 1.046))[23] or lead (^{207}Pb (22.1%, I = 1/2, μ_N = 0.5926))[23] (Fig. 6). The EPR spectra parameters for cations $\mathbf{1}^+$–$\mathbf{5}^+$ are summarized in Table 5.

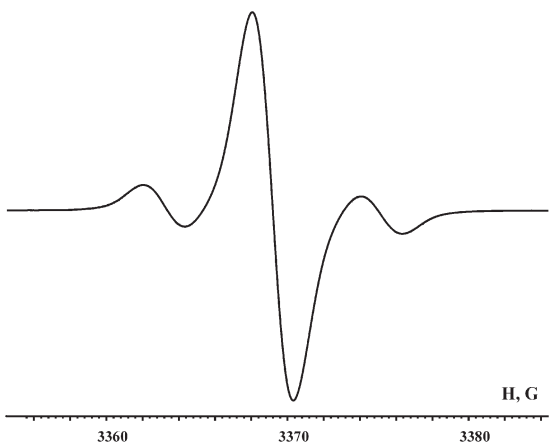

Fig. 6 An EPR spectrum of $\mathbf{5}^+$ in CH_2Cl_2 at 290 K.

Table 5 EPR spectra parameters[a] for cations $\mathbf{1}^+$–$\mathbf{5}^+$

Cation	$a_i(M^b)$, G	ΔH, G	g_i
$\mathbf{1}^+$	—[c]	2.55	2.0058
$\mathbf{2}^+$	5.80, 5.54	3.00	2.0042
$\mathbf{3}^+$	9.20, 8.80	2.85	2.0026
$\mathbf{4}^+$	6.80, 6.50	1.90	2.0035
$\mathbf{5}^+$	12.2	2.06	2.0032

[a] CH_2Cl_2. T = 290 K. [b] M = ^{119}Sn, ^{117}Sn for $\mathbf{1}^+$–$\mathbf{4}^+$ and M = ^{207}Pb for $\mathbf{5}^+$. [c] The satellite splitting in the EPR spectra of $\mathbf{1}^+$ is too small for clear determination and appears as shoulders on the central line.

The EPR spectra of anions $\mathbf{1}^{-}$–$\mathbf{4}^{-}$ are well resolved. They are quintets (1 : 2 : 3 : 2 : 1) of triplets (1 : 2 : 1) of quintets (1 : 4 : 6 : 4 : 1) with satellite splitting. The hyperfine structure of the EPR spectra of anions $\mathbf{1}^{-}$–$\mathbf{4}^{-}$ arises from the hyperfine coupling of unpaired electron with two and four equivalent magnetic ^{1}H nuclei (99.98%, $I = \frac{1}{2}$, $\mu_N = 2.7928$),[23] two equivalent nitrogen nuclei ^{14}N (99.63%, $I = 1$, $\mu_N = 0.4037$)[23] and the magnetic isotopes of tin ^{117,119}Sn (Fig. 7). The EPR spectra parameters for anions $\mathbf{1}^{-}$–$\mathbf{4}^{-}$ are summarized in Table 6. We were unable to obtain under the EPR experimental conditions stable paramagnetic derivative $\mathbf{5}^{-}$.

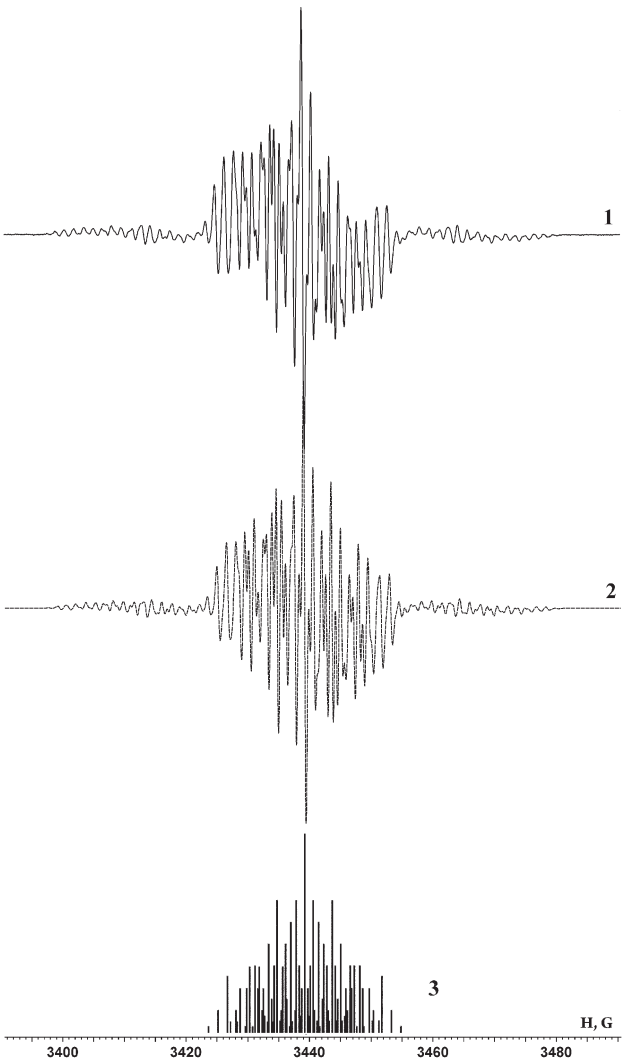

Fig. 7 The experimental EPR spectrum of $\mathbf{1}^{-}$ (1), its simulation (2) and stick-diagram (3) (^{117,119}Sn satellite splitting is omitted for the stick-diagram). $T = 290$ K, THF.

Table 6 EPR spectra parameters[a] for anions $\mathbf{1}^{-}$–$\mathbf{4}^{-}$

	$a_i(2^{14}N)$/G	$a_i(2^{1}H)$/G	$a_i(4^{1}H)$/G	$a_i(^{119,117}Sn)$/G	g_i
$\mathbf{1}^{-}$	4.44	3.56	1.54	51.10, 48.80	2.0024
$\mathbf{2}^{-}$	4.47	3.47	1.53	56.20, 53.72	2.0025
$\mathbf{3}^{-}$	4.46	3.54	1.56	65.40, 62.50	2.0026
$\mathbf{4}^{-}$	4.48	3.49	1.58	43.20, 41.30	2.0019

[a] THF, $T = 290$ K.

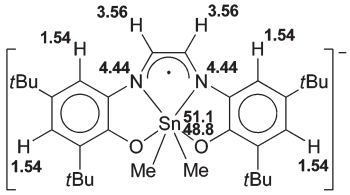

Scheme 4 The assignment of *hfs* constants in $\mathbf{1}^{-}$. The *hfs* constants are given in Gauss.

The hyper fine splitting (*hfs*) constants with magnetic isotopes ^{119,117}Sn in the EPR spectra of anions $\mathbf{1}^{-}$–$\mathbf{4}^{-}$ are four times lower than the values characteristic for tin(II) derivatives with paramagnetic ligands[24] and lie in the same region as for *o*-iminosemiquinolate tin(IV) complexes.[18b,d] It unequivocally confirms that the reduction of complexes **1**–**4** does not concern the metallic center.

The *hfs* with two equivalent protons $a_i(2H) = 3.47$–3.56 G in EPR spectra of anions $\mathbf{1}^{-}$–$\mathbf{4}^{-}$ should to be attributed to the protons of the glyoxal fragment. The values of *hfs* constants on two equivalent nitrogen atoms in anions $\mathbf{1}^{-}$–$\mathbf{4}^{-}$ are slightly lower than those observed for tin derivatives containing the radical-anion of diazabutadiene.[24] It indicates that most of the spin density in $\mathbf{1}^{-}$–$\mathbf{4}^{-}$ is localized on the glyoxal fragment of the ligand. The delocalization of spin density into the two phenolic moieties of the ligand calls for the additional *hfs* with four equivalent protons with constants $a_i(4H) \approx 1.5$ G. The assignment of *hfs* constants in $\mathbf{1}^{-}$ is depicted in Scheme 4. Thus anions $\mathbf{1}^{-}$–$\mathbf{4}^{-}$ have to be considered as containing a trianion of the L ligand in the L^{-3B} rather than L^{-3A} resonance form (Scheme 1).

DFT calculations

We have performed DFT calculations for complex **1** and its pyridine adduct **1**·**Py** in the closed-shell singlet ground state. The doublet cation and anion of **1** were computed also. The optimized structural parameters are given in Table 7 along with the corresponding experimental values (atom labelling follows that in the crystal structure, see Fig. 1).

It is seen that the calculated structural parameters are in good agreement with the experimental values. Though the trends in C–C bond lengths are well described by the chosen level of theory, the Sn–N, Sn–O and Sn–C bond lengths are slightly overestimated. Computations of **1**, **1**·**Py**, $\mathbf{1}^{-}$ and $\mathbf{1}^{+}$ were performed with no symmetry restrictions but all optimized structures have a two-fold axis passing through the tin atom and the middle of the C(15)–C(16) bond. The optimized L ligand in **1**, **1**·**Py**, $\mathbf{1}^{-}$ and $\mathbf{1}^{+}$ is planar.

The redox activity of complex **1** is specified with frontier orbitals. The HOMO (−5.07 eV), HOMO-1 (−5.77 eV) and HOMO-2 (−6.44 eV) orbitals are localized on the L ligand and they contain no contribution of the tin atom (Fig. 8).

The HOMO-3 (−6.75 eV) is the highest occupied orbital responsible for metal–ligand bonding in the complex. The LUMO (−3.16 eV) is a ligand-localized orbital. Its small part

Table 7 Experimental bond distances (Å) and angles (°) of **1** in comparison with the calculated values for **1**, **1**·**Py**, $\mathbf{1}^-$ and $\mathbf{1}^+$

Bond	**1** (Exp.)	**1** (Calc.)	**1**·**Py**	$\mathbf{1}^-$	$\mathbf{1}^+$
Sn(1)–O(1)	2.2518(16)	2.285	2.285	2.316	2.349
Sn(1)–N(1)	2.2626(19)	2.304	2.390	2.252	2.296
O(1)–C(1)	1.295(3)	1.299	1.306	1.311	1.272
N(1)–C(15)	1.301(3)	1.315	1.307	1.344	1.337
N(1)–C(2)	1.386(3)	1.378	1.380	1.388	1.360
C(1)–C(2)	1.426(3)	1.443	1.440	1.441	1.475
C(1)–C(6)	1.439(3)	1.446	1.445	1.433	1.458
C(2)–C(3)	1.410(3)	1.416	1.415	1.407	1.414
C(3)–C(4)	1.371(3)	1.381	1.382	1.396	1.381
C(4)–C(5)	1.426(3)	1.428	1.424	1.412	1.445
C(5)–C(6)	1.372(3)	1.385	1.387	1.399	1.373
C(15)–C(16)	1.419(3)	1.429	1.437	1.399	1.402
Sn(1)–C(31)	2.115(2)	2.166	2.178	2.174	2.157
Sn(1)–N(Py)			2.554		
Angle					
O(1)–Sn(1)–O(2)	146.12	146.55	152.03	144.77	149.05
N(1)–Sn(1)–N(2)	71.78	71.77	69.03	73.09	72.24
C(31)–Sn(1)–C(32)	144.75	148.74	174.90	142.00	144.05

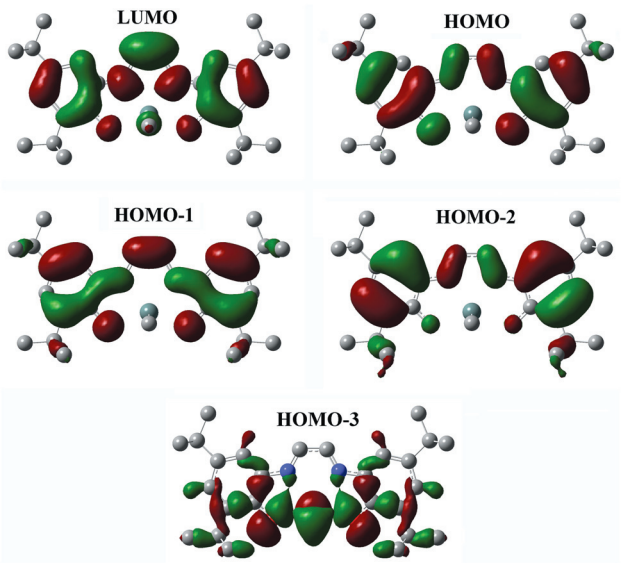

Fig. 8 Representation of the frontier orbitals, HOMO-1, HOMO-2 and HOMO-3 of **1** from the DFT calculation (the isovalue is 0.02 a.u.). H atoms are omitted for clarity.

formed by the Sn and Me contributions is antibonding for the Sn–Me bond. The HOMO–LUMO gap (1.92 eV) is in reasonable agreement with the experimental values which can be estimated from the electrochemical (1.48 eV) or UV-vis spectroscopy (1.57 eV for the long-wavelength band) experiments. The second intense band in the UV-visible spectrum at ~400 nm (~3.1 eV) for complex **1** should be attributed to the another intraligand HOMO-2–LUMO (3.28 eV) transition.

The coordination of the pyridine molecule to the tin atom leads to the weakening of the metal–glyoxal coordination in **1**·**Py**. This results in elongation of the Sn–N(glyoxal) bonds followed by redistribution of bond distances in the glyoxal fragment which tend towards the free diimine values. Pyridine coordination causes an increase of the Me–Sn–Me angle by 30°. This

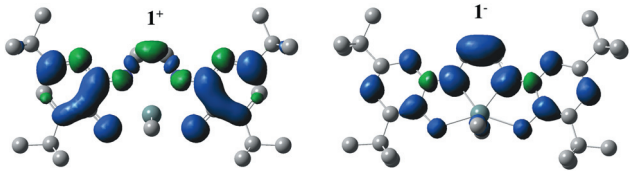

Fig. 9 Spin density isosurfaces for cation $\mathbf{1}^+$ (left) and anion $\mathbf{1}^-$ (right). The isovalue is 0.0015 a.u. H atoms are omitted for clarity.

distortion was predicted by the NMR spectroscopy experiments mentioned above. The shape of the frontier orbitals is not influenced by the pyridine coordination. At the same time the HOMO (−4.84 eV)–LUMO (−2.72 eV) and HOMO-2 (−6.18 eV)–LUMO (−2.72 eV) gaps (2.12 and 3.46 eV respectively) increase in comparison with the six-coordinated complex **1**. This accounts for a hypsochromic shift in the electronic absorption spectra of **1** in coordinating solvents.

The reduction of **1** is accompanied with population of the LUMO. The bond distance redistribution affects both the phenolic and glyoxal part of the ligand. The quinoid-type distortion in the two phenolic parts disappears while the C–C and C–N bond distances of the glyoxal fragment (1.400 and 1.344 Å respectively) become very close to those obtained for the diimine radical-anion.[16] The Me_2Sn moiety moves into the chelate ONNO semi-ring during the reduction of complex **1** which is clear from the Sn–O and Sn–N bond lengths changing. It leads to an increase in sterical hindrance around the metal atom in $\mathbf{1}^-$. This effect, along with the population of the antibonding orbital for the M–C bond, accounts for the instability (according to the EPR and electrochemical experiments) of anions $\mathbf{3}^-$ and $\mathbf{5}^-$ containing bulky substituents at the metal atom. The spin density in the anion $\mathbf{1}^-$ is essentially localized on the NCCN fragment (Fig. 9). The Mulliken spin densities on both the N and C atoms are 0.22 and 0.12 respectively.

The isotropic Fermi constants from the DFT calculations ($a_i(^{2}^{14}N)$ = 5.7 G, $a_i(^{2}^{1}H)$ = 3.5 G, $a_i(^{2}^{1}H)$ = 1.8 G, $a_i(^{2}^{1}H)$ = 1.9 G, $a_i(^{117}Sn)$ = 48.1 G) are in good agreement with the *hfs* constants obtained in the EPR experiment. Thus the calculations confirm the anion $\mathbf{1}^-$ structure as that containing an L trianion ligand in the L^{-3B} resonance form (Scheme 1).

The oxidation of **1** is accompanied by the sharpening of the quinoid-type distortion in the two phenolic rings. The C(1)–O(1), C(2)–C(3) and C(5)–C(6) bonds of $\mathbf{1}^+$ are shorter in comparison with neutral **1**. The examination of the spin distribution (Fig. 9) in cation $\mathbf{1}^+$ demonstrates that the unpaired electron is delocalized between two phenoxy moieties of the ligand predominantly. The Mulliken spin densities on the O(1), C(2), C(4) and C(6) atoms are 0.17, 0.19, 0.19 and 0.06 respectively. Such a spin distribution in cation $\mathbf{1}^+$ leads to the small hyperfine coupling of the unpaired electron with the hydrogen and nitrogen atoms of both the phenolic and glyoxal parts of the ligand. As a result the hyperfine structure in the EPR spectrum of $\mathbf{1}^+$ is absent.

Conclusions

We reported the first examples of metal complexes containing a tetradentate redox active ligand – glyoxal-bis(2-hydroxy-3,5-di-

tert-butylanil). Complexes **1–5** give the unique opportunity to investigate the redox behavior of this ligand which is not complicated by redox transformations of the metallic center. The possibility of the dianionic form of the ligand undergoing redox transformations was shown using electrochemistry, EPR spectroscopy and DFT calculations.

Acknowledgements

We are grateful to the FSP "Scientific and Scientific-Pedagogical Cadres of Innovation Russia" for 2009–2013 years (GK P839 from 25.05.2010), Russian Foundation for Basic Research (grant 11-03-97041-r_povolzh'e_a, 12-03-00513-a), Russian President Grants (NSh-1113.2012.3, MK-614.2011.3, MK-1156.2011.3) for financial support of this work.

References

1 (*a*) C. G. Pierpont, *Coord. Chem. Rev.*, 2001, **219–221**, 415–433; (*b*) C. G. Pierpont, *Coord. Chem. Rev.*, 2001, **216–217**, 99–125; (*c*) A. I. Poddelsky, V. K. Cherkasov and G. A. Abakumov, *Coord. Chem. Rev.*, 2009, **253**, 291–324.
2 A. V. Piskunov and A. I. Poddel'sky, *Glob. J. Inorg. Chem.*, 2011, **2**, 110–149.
3 (*a*) G. A. Abakumov, A. I. Poddel'sky, E. V. Grunova, V. K. Cherkasov, G. K. Fukin, Yu. A. Kurskii and L. G. Abakumova, *Angew. Chem., Int. Ed.*, 2005, **44**, 2767–2771; (*b*) V. K. Cherkasov, G. A. Abakumov, E. V. Grunova, A. I. Poddel'sky, G. K. Fukin, E. V. Baranov, Yu. A. Kursky and L. G. Abakumova, *Chem.–Eur. J.*, 2006, **12**, 3916–3927; (*c*) A. V. Lado, A. V. Piskunov, V. K. Cherkasov, G. K. Fukin and G. A. Abakumov, *Russ. J. Coord. Chem.*, 2006, **32**, 173–180; (*d*) E. V. Kolyakina, L. B. Vaganova, A. V. Piskunov, A. V. Lado, V. K. Cherkasov and D. F. Grishin, *Polym. Sci. Ser. A*, 2008, **50**, 153–159; (*e*) A. V. Piskunov, I. N. Mescheryakova, G. K. Fukin, E. V. Baranov, M. Hummert, A. S. Shavyrin, V. K. Cherkasov and G. A. Abakumov, *Chem.–Eur. J.*, 2008, **14**, 10085–10093; (*f*) I. L. Fedushkin, A. S. Nikipelov and K. A. Lyssenko, *J. Am. Chem. Soc.*, 2010, **132**, 7874–7875; (*g*) I. L. Fedushkin, A. S. Nikipelov, A. G. Morozov, A. A. Skatova, A. V. Cherkasov and G. A. Abakumov, *Chem.–Eur. J.*, 2012, **18**, 255–266.
4 (*a*) P. Chaudhuri, M. Hess, J. Müller, K. Hildenbrand, E. Bill, T. Weyhermüller and K. Wieghardt, *J. Am. Chem. Soc.*, 1999, **121**, 9599–9610; (*b*) K. J. Blackmore, N. Lal, J. W. Ziller and A. F. Heyduk, *J. Am. Chem. Soc.*, 2008, **130**, 2728–2729; (*c*) A. L. Zelikoff, J. Kopilov, I. Goldberg, G. W. Coatesb and M. Kol, *Chem. Commun.*, 2009, 6804–6806; (*d*) K. J. Blackmore, N. Lal, J. W. Ziller and A. F. Heyduk, *Eur. J. Inorg. Chem.*, 2009, 735–743.
5 P. Ghosh, E. Bill, E. Bothe, T. Weyhermüller, F. Neese and K. Wieghardt, *J. Am. Chem. Soc.*, 2003, **125**, 1293–1308.
6 A. S. Roy, N. Muresan, H. M. Tuononen, S. P. Rathd and P. Ghosh, *Dalton Trans.*, 2008, 3438–3446.
7 H. Haeussler and H. Jadamus, *Chem. Ber.*, 1964, **97**, 3051–3055.
8 K. S. Min, T. Weyhermüller, E. Bothe and K. Wieghardt, *Inorg. Chem.*, 2004, **43**, 2922–2931.
9 D. D. Perrin, W. L. F. Armarego and D. R. Perrin, *Purification of Laboratory Chemicals*, Pergamon, Oxford, 1980.
10 K. A. Kocheshkov, N. N. Zemlyanskii, N. I. Sheverdina and E. M. Panov, *Methods of Elementoorganic Chemistry. Germanium, Tin, Lead*, Nauka, Moscow, 1968, p. 704.
11 Bruker, *SAINTPLUS Data Reduction and Correction Program v.6.02a*, Bruker AXS, Madison, WI, USA, 2000.
12 G. M. Sheldrick, *SADABS v.2.01, Bruker/Siemens Area Detector Absorption Correction Program*, Bruker AXS, Madison, WI, USA, 1998.
13 G. M. Sheldrick, *SHELXTL v.6.12, Structure Determination Software Suite*, Bruker AXS, Madison, WI, USA, 2000.
14 M. J. Frisch, G. W. Trucks, H. B. Schlegel, M. J. Frisch, G. W. Trucks, H. B. Schlegel, G. E. Scuseria, M. A. Rob, J. R. Cheeseman, J. A. Montgomery, Jr., T. Vreven, K. N. Kudin, J. C. Burant, J. M. Millam, S. S. Iyengar, J. Tomasi, V. Barone, B. Mennucci, M. Cossi, G. Scalmani, N. Rega, G. A. Petersson, H. Nakatsuji, M. Hada, M. Ehara, K. Toyota, R. Fukuda, J. Hasegawa, M. Ishida, T. Nakajima, Y. Honda, O. Kitao, H. Nakai, M. Klene, X. Li, J. E. Knox, H. P. Hratchian, J. B. Cross, V. Bakken, C. Adamo, J. Jaramillo, R. Gomperts, R. E. Stratmann, O. Yazyev, A. J. Austin, R. Cammi, C. Pomelli, J. W. Ochterski, P. Y. Ayala, K. Morokuma, G. A. Voth, P. Salvador, J. J. Dannenberg, V. G. Zakrzewski, S. Dapprich, A. D. Daniels, M. C. Strain, O. Farkas, D. K. Malick, A. D. Rabuck, K. Raghavachari, J. B. Foresman, J. V. Ortiz, Q. Cui, A. G. Baboul, S. Clifford, J. Cioslowski, B. B. Stefanov, G. Liu, A. Liashenko, P. Piskorz, I. Komaromi, R. L. Martin, D. J. Fox, T. Keith, M. A. AllLaham, C. Y. Peng, A. Nanayakkara, M. Challacombe, P. M. W. Gill, B. Johnson, W. Chen, M. W. Wong, C. Gonzalez and J. A. Pople, *Gaussian 03, Revision A.1*, Gaussian, Inc., Pittsburgh (PA), 2003.
15 A. V. Piskunov, A. V. Lado, G. K. Fukin, E. V. Baranov, L. G. Abakumova, V. K. Cherkasov and G. A. Abakumov, *Heteroat. Chem.*, 2006, **17**, 481–490.
16 M. G. Gardiner, G. R. Hanson, M. J. Henderson, F. C. Lee and L. C. Raston, *Inorg. Chem.*, 1994, **33**, 2456.
17 T. Glaser, M. Heidemeier and T. Lugger, *J. Chem. Soc., Dalton Trans.*, 2003, 2381.
18 (*a*) A. V. Piskunov, I. A. Aivaz'yan, G. K. Fukin, E. V. Baranov, A. S. Shavyrin, V. K. Cherkasov and G. A. Abakumov, *Inorg. Chem. Commun.*, 2006, **9**, 612–615; (*b*) A. V. Piskunov, I. A. Aivaz'yan, G. A. Abakumov, V. K. Cherkasov, O. V. Kuznetsova, G. K. Fukin and E. V. Baranov, *Russ. Chem. Bull.*, 2007, **56**, 261–266; (*c*) A. V. Lado, A. I. Poddel'sky, A. V. Piskunov, G. K. Fukin, E. V. Baranov, V. N. Ikorskii, V. K. Cherkasov and G. A. Abakumov, *Inorg. Chim. Acta*, 2005, **358**, 4443–4450; (*d*) A. V. Piskunov, I. N. Mescheryakova, E. V. Baranov, G. K. Fukin, V. K. Cherkasov and G. A. Abakumov, *Russ. Chem. Bull.*, 2010, **59**, 361–370; (*e*) A. V. Piskunov, I. N. Mescheryakova, G. K. Fukin, G. V. Romanenko, A. S. Bogomyakov, V. K. Cherkasov and G. A. Abakumov, *Heteroat. Chem.*, 2009, **20**, 332–340.
19 (*a*) J. Otera, *J. Organomet. Chem.*, 1981, **221**, 57; (*b*) D. K. Dey, M. K. Das and R. K. Bansal, *J. Organomet. Chem.*, 1997, **535**, 7.
20 J. Holecek, M. Nadvornik, K. Handlir and A. Lycka, *J. Organomet. Chem.*, 1983, **241**, 177.
21 T. P. Lockhart and W. F. Manders, *Inorg. Chem.*, 1986, **25**, 892–895.
22 I. V. Smolyaninov, N. N. Letichevskaya, A. V. Kulakov, Ya. B. Aref'ev, K. P. Pashchenko and N. T. Berberova, *Russ. J. Electrochem.*, 2007, **43**, 1187–1199.
23 J. Emsley, *The Elements*, Clarendon Press, Oxford, 1991.
24 (*a*) G. A. Abakumov, V. K. Cherkasov, A. V. Piskunov and N. O. Druzhkov, *Dokl. Chem.*, 2004, **399**, 233–255; (*b*) A. V. Piskunov, A. I. Aivaz'yan, V. K. Cherkasov and G. A. Abakumov, *J. Organomet. Chem.*, 2006, **691**, 1531–1534.